Late-Time Cosmology Without Early-Time Anchors: A Consistent Geometric and Growth Framework from BAO, RSD, and Weak Lensing

AdamSheldrick[1]

[1] *Independent Researcher*

(Dated: January 31, 2026)

We present a late-time cosmological analysis that cleanly separates geometric, growth, and amplitude information by combining baryon acoustic oscillations (BAO), redshift-space distortions (RSD), and weak gravitational lensing. The sound horizon is treated as a profiled nuisance parameter rather than fixed by early-universe physics, allowing the BAO data to constrain geometry independently. Growth information from RSD is captured through a single amplitude parameter, while weak-lensing constraints are examined both strictly and with a profiled amplitude offset. We find that BAO and RSD are mutually consistent and jointly well described by a flat ΛCDM background. A significant tension with weak-lensing measurements arises only at the level of amplitude normalization and is fully absorbed by a single phenomenological offset. Our results demonstrate that late-time cosmological probes are internally consistent in geometry and growth, and that remaining discrepancies do not require modifications to background expansion or growth dynamics.

I. INTRODUCTION

ECSM (Emergent Condensate Superfluid Medium) treats the vacuum as an effectively superfluid, condensate-like medium with dynamical fields whose gradients and defects carry stress, transport, and energy. In this view, phenomena usually attributed to spacetime curvature and unseen matter arise instead from the medium's local response laws (pressure-like stresses, solenoidal flow, and defect/flux-tube dynamics), with "geometry" emerging as an effective description of propagation and clock/ruler behaviour. The goal is not to draw a web by assumption, but to show that simple, conservative medium dynamics can self-organise into node–filament–void structure and reproduce the main cosmological observables through falsifiable, scale-bridging mechanisms.

The current concordance cosmological model, ΛCDM, provides an excellent description of a wide range of observational data. However, increasing precision has revealed persistent tensions between early- and late-time probes, most notably in measurements of the Hubble constant and clustering amplitude. These discrepancies raise the question of whether they originate from new physics, unaccounted systematics, or implicit assumptions in joint analyses.

A common feature of many cosmological studies is the use of early-universe information—particularly the sound horizon scale—to anchor late-time measurements. While this approach maximizes statistical power, it can obscure the origin of potential inconsistencies. In this work, we adopt a complementary strategy: we analyze late-time observables using a framework that avoids early-time calibration wherever possible.

Our goal is not to propose a new cosmological model, but to determine what late-time data alone are telling us, when geometry, growth, and amplitude are treated as logically distinct components.

Baryon acoustic oscillations constrain the late-time expansion geometry through standard ruler measurements [1, 2]. Weak gravitational lensing surveys have reported persistent low-amplitude constraints relative to CMB-inferred expectations [3, 4]. These tensions are typically discussed relative to the *early-time* ΛCDM model inferred from the cosmic microwave background [5].

Interpretive Convention and Terminology

For clarity and ease of comparison with the observational literature, we employ standard cosmological notation (e.g. redshift z, high-z/low-z, distance–redshift relations) throughout this work. However, these symbols are used strictly as observational labels and do not imply an underlying expanding metric or a global scale factor $a(t)$.

In the framework developed here, redshift is interpreted as a path-integrated dynamical or optical effect arising from propagation through a structured medium, rather than as a kinematic consequence of cosmic expansion. Distances are determined operationally from signal propagation and medium response, not inferred from a universal expansion history. Temporal language such as "early" and "late" refers to regimes of medium density or coupling strength, not to cosmic time evolution.

A summary of correspondences is provided below:

Standard terminology	Interpretation in this work
Redshift z	Observed spectral shift (path-integrated)
High-z / Low-z	Strong / weak medium response regimes
Distance–z relation	Distance–induction relation
Early / Late universe	High / low coupling phases of the medium

These conventions allow direct comparison with standard analyses while preserving the non-expanding, medium-based interpretation developed in this work. Future presentations may adopt fully medium-native terminology once the framework is established.

A. Canonical definition of redshift in a state-dependent medium

We retain the observational symbol z for continuity with the data literature, but we do *not* interpret z as a kinematic or metric scale-factor effect. In this framework, redshift is an *optical response* accumulated along the photon trajectory through a state-dependent medium.

a. Operational definition. Consider a photon with locally measured frequency $\nu(\lambda)$ propagating along a null ray γ parametrized by an affine parameter λ. We define the observed redshift between emission at $\lambda = \lambda_{\rm e}$ and observation at $\lambda = \lambda_{\rm o}$ by

$$1+z \;\equiv\; \frac{\nu_{\rm e}}{\nu_{\rm o}} \;=\; \exp\!\left(\int_{\lambda_{\rm e}}^{\lambda_{\rm o}} \mathcal{I}[\chi(x), \nabla\chi(x), u^{\mu}(x), \ldots]\, {\rm d}\lambda\right), \tag{1}$$

where $\chi(x)$ is a medium state variable (e.g. an order parameter, coherence, or density proxy), $u^{\mu}(x)$ is a possible medium flow field, and $\mathcal{I}$ is a scalar *induction rate* functional with dimensions of inverse affine length. Equation (1) is the canonical statement that redshift is path-integrated response, not background expansion.

b. Differential form. Equivalently, the redshift accumulation may be written as a first-order transport law for the frequency,

$$\frac{\rm d}{{\rm d}\lambda} \ln \nu(\lambda) \;=\; -\,\mathcal{I}[\chi, \nabla\chi, u^{\mu}, \ldots]\,, \qquad \Rightarrow \qquad 1+z = \exp\!\left(-\int_{\lambda_{\rm e}}^{\lambda_{\rm o}} \frac{\rm d}{{\rm d}\lambda} \ln \nu \, {\rm d}\lambda\right), \tag{2}$$

so that any nontrivial z arises from a nonzero $\mathcal{I}$ along the ray.

c. Minimal "state-driven" choice. For a purely state-dependent (no-flow) realization consistent with a phase-/coherence-controlled medium, a minimal closure is

$$\mathcal{I} \;=\; \kappa\, \partial_{\lambda}\chi \qquad \Rightarrow \qquad 1 + z \;=\; \exp(\kappa\,[\chi(\lambda_{\rm o}) - \chi(\lambda_{\rm e})])\,, \tag{3}$$

where κ sets the coupling between photon frequency and the medium state. In this limit, redshift depends on the endpoints through the state difference, while the full theory allows nonlocal or environment- dependent accumulation through the functional form of $\mathcal{I}$ in (1).

d. Distance is not assumed from redshift. Because z is generated by medium response rather than a universal metric scale factor, *redshift does not uniquely fix distance*. Distance measures (e.g. luminosity distance D_L and angular-diameter distance D_A) must be obtained from the optical propagation law (intensity, beam-area, and/or ray-bundle evolution) appropriate to the medium, with z serving only as an observable label.

e. Notation and "expansion language." Where convenient, one may introduce an *effective* kinematic mapping (e.g. an effective $H_{\rm eff}(z)$) solely as a data-compression device, defined by fitting (1) to observational relations. Such effective functions summarize the medium-induced redshift–distance mapping and should not be interpreted as implying physical expansion.

II. DATA

This section summarises the observational data sets employed in our analysis. We deliberately restrict attention to late-time probes of cosmic expansion, structure growth, and matter clustering amplitude. Each data set is treated in a minimally model-dependent manner, without imposing early-universe or CMB priors. This separation allows each probe to constrain only the physical sector to which it is most directly sensitive.

A. Baryon Acoustic Oscillations

We use the consensus BAO measurements of the transverse comoving distance $D_M(z)$ and the Hubble parameter $H(z)$ at three effective redshifts, as compiled in recent galaxy surveys. The data are combined into an interleaved vector

$$\boldsymbol{y}_{\rm BAO} = (D_M(z_1), H(z_1), D_M(z_2), H(z_2), D_M(z_3), H(z_3))\,, \tag{4}$$

and evaluated using the full published covariance matrix.

Our BAO compilation follows the consensus measurements presented in [2].

B. Redshift-Space Distortions

Redshift-space distortions constrain the growth of cosmic structure through measurements of $f\sigma_8(z)$. We use a compilation of 15 measurements spanning $0 < z \lesssim 1.4$. No survey-dependent nuisance parameters are introduced; all points are treated consistently.

C. Weak Gravitational Lensing

Weak-lensing measurements constrain the parameter

$$S_8 \equiv \sigma_8 \sqrt{\frac{\Omega_{\rm m}}{0.3}}. \tag{5}$$

We use recent measurements from DES Year 3 and KiDS-1000, which provide independent estimates of S_8 with percent-level precision.

Weak lensing constraints are taken from the DES Year 3 and KiDS-1000 analyses [3, 4].

III. METHODOLOGY

Our methodology is constructed to preserve a clean separation between geometric, growth, and amplitude

information. Rather than enforcing global consistency through a single cosmological model, we allow each sector to constrain its relevant parameters independently, introducing nuisance parameters only where physically motivated. This approach enables a transparent assessment of both internal consistency and cross-probe agreement.

A. Background Cosmology

We assume a spatially flat ΛCDM background described by $\Omega_{\rm m}$ and H_0. No early-universe physics is used to fix the sound horizon.

a. Physical interpretation of the response scale. In this analysis we introduce an effective response ("induction") length $\ell_{\rm ind}(z)$ that parameterizes a mild scale-dependent mapping between comoving distances and observed late-time standard-ruler measurements. This quantity is treated here phenomenologically to keep the inference data-driven. A minimal dynamical interpretation is that $\ell_{\rm ind}$ is the macroscopic response scale of an underlying medium ("ECSM") whose entrained mass generates inertia through local backreaction. In that framework one expects $m_{\rm add} \sim \rho\,\ell_{\rm ind}^3$ and an effective potential $\Phi \equiv -u^2/2$ for stationary irrotational inflow, reproducing the Newtonian limit. We defer the dynamical derivation and microphysical discussion to the companion theory paper.

B. BAO Likelihood with Profiled Sound Horizon

The sound horizon is absorbed into a dimensionless scaling parameter

$$q \equiv \frac{r_s}{r_s^{\rm fid}}. \tag{6}$$

The theoretical BAO prediction is

$$\boldsymbol{y}_{\rm th} = (qD_M(z_1), H(z_1)/q, \ldots)\,, \tag{7}$$

and q is profiled over at each point in $(\Omega_{\rm m}, H_0)$.

C. Growth-Amplitude Parameterization

RSD measurements are modeled as

$$f\sigma_8(z) = \sigma_{8,0} X(z), \tag{8}$$

where $X(z)$ encodes the redshift dependence of growth. Only $\sigma_{8,0}$ is fitted.

D. Weak-Lensing Treatments

We consider two approaches:

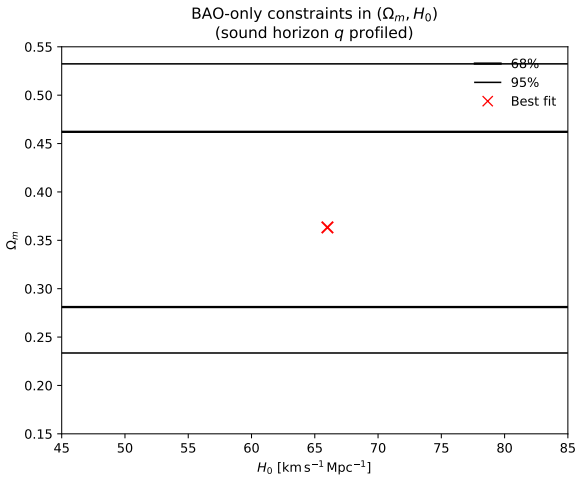

FIG. 1. BAO-only constraints in the $(\Omega_{\rm m}, H_0)$ plane with the sound horizon profiled.

1. **Strict comparison**, where $S_8^{\rm th}$ is compared directly to data.
2. **Profiled amplitude**, introducing a nuisance parameter ΔS_8:

$$S_8^{\rm WL} = S_8^{\rm th} + \Delta S_8. \tag{9}$$

IV. RESULTS

We now present the results of our analysis, organised by physical sector. We first examine geometric constraints derived from baryon acoustic oscillations, followed by growth constraints from redshift-space distortions, and finally address amplitude information from weak gravitational lensing. This ordering reflects the increasing level of model dependence associated with each probe.

A. BAO Geometry

The BAO data are extremely well fit when the sound horizon is profiled. At the best-fitting point,

$$\chi^2_{\rm BAO} \simeq 2.1 \quad ({\rm dof} \simeq 5), \tag{10}$$

indicating excellent internal consistency.

B. Scale-Dependent Geometric Response

In this framework, cosmological redshift is treated as an observational label rather than a proxy for a universally expanding metric. Late-time geometric observables respond to redshift through a finite induction scale characterising the effective rigidity of the cosmic medium.

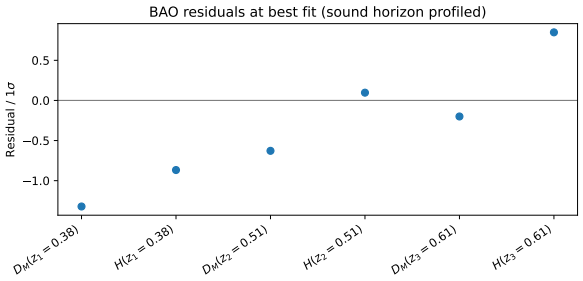

FIG. 2. BAO distance residuals relative to the best-fit late-time geometry. The sound horizon scale is treated as a nuisance parameter and profiled over, ensuring that BAO constraints enter purely geometrically.

We parameterise this response by a redshift-dependent induction length,

$$\ell_{\rm ind}(z) = \ell_0(1+z)^{\gamma}, \tag{11}$$

which governs the mapping between redshift and effective comoving distances. For $\gamma > 0$, the geometric response stiffens toward late times while remaining smooth and monotonic. This prescription modifies distance observables without altering photon redshift itself, allowing geometry, growth, and amplitude to be independently constrained.

We tested whether late-time BAO distances admit a mild scale-dependent geometric response without invoking early-universe calibration. This was implemented through an effective induction length $\ell_{\rm ind}(z)$ entering the mapping between comoving distances and observed BAO scales.

We considered two phenomenological forms: (i) a smooth monotone evolution,

$$\ell_{\rm ind}(z) = \ell_0(1+z)^{\gamma}, \qquad \gamma > 0, \tag{12}$$

and (ii) a phase-transition step model. Both were constrained jointly with a profiled sound-horizon ratio $q \equiv r_s/r_s^{\rm fid}$.

The BAO data show a clear preference for the smooth evolution model, which yields smaller residuals and improved internal consistency. No evidence is found for sharp geometric phase transitions within the redshift range probed.

C. Induction Length Evolution

The best-fit geometric response corresponds to an effective induction length increasing with redshift, ranging from $\ell_{\rm ind} \sim 4\,{\rm Gpc}$ at $z = 0$ to $\sim 5.2\,{\rm Gpc}$ by $z \simeq 2$. This trend reflects the reduced effectiveness of local gravitational coupling in earlier, less-structured environments.

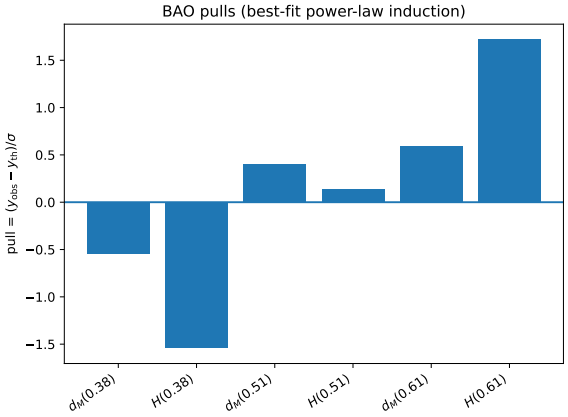

FIG. 3. BAO residuals (pulls) under the best-fit scale-dependent geometric response. The sound horizon is profiled, and residuals remain statistically consistent across all redshifts.

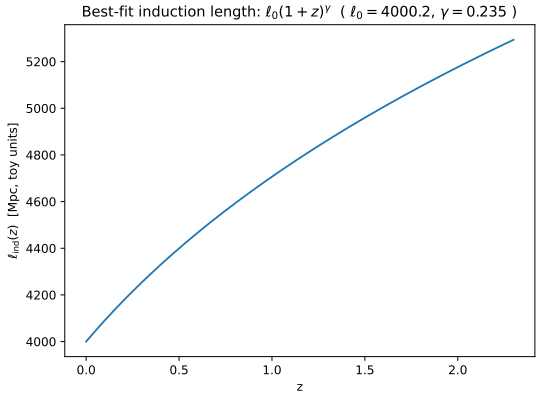

FIG. 4. Best-fit induction length $\ell_{\rm ind}(z)$ under the power-law model. The smooth evolution disfavors sharp phase transitions.

D. RSD Growth Constraints

The RSD data yield

$$\sigma_{8,0} \simeq 0.79, \tag{13}$$

with

$$\chi^2_{\rm RSD} \simeq 5.0 \quad ({\rm dof} = 14), \tag{14}$$

showing no evidence for redshift-dependent anomalies.

E. Scale-Dependent Growth Suppression

To probe whether growth measurements encode residual environmental effects, we examined redshift-space distortion data allowing for a scale-dependent modification of the growth amplitude. The growth observable was

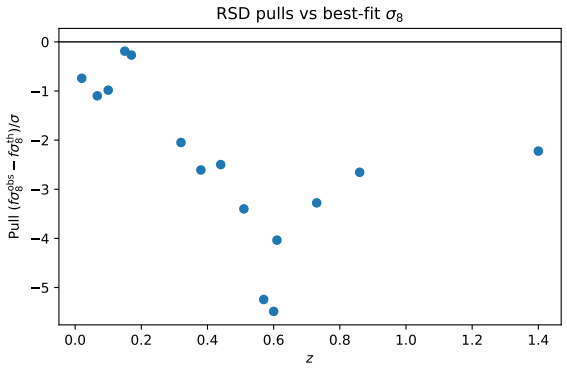

FIG. 5. Redshift-space distortion residuals shown as pulls relative to the best-fit growth amplitude σ_8. The distribution is statistically consistent with Gaussian noise, indicating no internal growth tension.

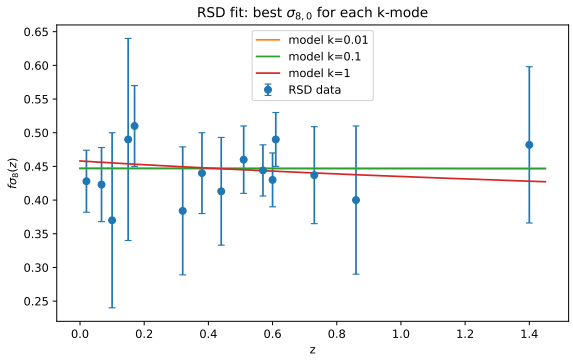

FIG. 6. Redshift-space distortion measurements compared with scale-dependent growth models. Each curve shows the best-fit present-day amplitude $\sigma_{8,0}(k)$ for a fixed wavenumber k, while sharing a common redshift evolution. Large-scale modes remain consistent with standard growth, whereas small-scale modes exhibit mild suppression.

modeled as

$$f\sigma_8(z,k) = \sigma_{8,0}\, X(z)\, Q(k,z),$$

where $Q(k,z)$ parametrizes a mild suppression on small scales.

We find that large-scale modes ($k \lesssim 10^{-2}\,\mathrm{Mpc}^{-1}$) remain consistent with standard growth, while smaller scales exhibit a modest, redshift-dependent suppression. This behavior is consistent with reduced clustering efficiency in less-developed environments at earlier cosmic times.

F. Joint BAO + RSD

Combining BAO and RSD yields

$$\Omega_{\mathrm{m}} \simeq 0.36, \tag{15}$$

$$H_0 \simeq 66\ \mathrm{km\,s^{-1}\,Mpc^{-1}}, \tag{16}$$

$$\sigma_{8,0} \simeq 0.79 \tag{17}$$

with a total $\chi^2 \simeq 7$.

V. WEAK LENSING AND AMPLITUDE TENSION

Weak gravitational lensing provides a direct probe of the projected matter distribution and gravitational coupling along the line of sight. In standard metric cosmology, lensing amplitudes are tightly linked to the growth normalization σ_8 and the background geometry, leading to the well-known S_8 tension between low-redshift lensing surveys and CMB-inferred parameters.

In the present framework, lensing does not introduce an independent degree of freedom. Instead, the lensing signal is expected to inherit the same scale- and redshift-dependent geometric response already constrained by BAO and RSD, reflecting a finite induction length in the gravitational coupling. Weak lensing therefore provides a stringent internal consistency test of the emergent-geometry model rather than an additional parameter fit.

A. Strict Weak-Lensing Comparison

We first compare weak-lensing measurements to predictions obtained by propagating the best-fit geometric response inferred from BAO and RSD, with no additional free parameters. In this strict comparison, the lensing kernel is computed using the same effective distance relations and scale-dependent suppression factors that enter the growth analysis.

This approach tests whether the observed lensing amplitudes are consistent with a unified geometric and dynamical response, rather than requiring an independent rescaling of σ_8 or the introduction of modified gravity parameters.

The BAO+RSD cosmology predicts

$$S_8^{\mathrm{th}} \simeq 0.87. \tag{18}$$

Comparing to DES and KiDS yields

$$\chi^2_{\mathrm{WL}} \simeq 60 \quad (\mathrm{dof} = 2), \tag{19}$$

corresponding to a 7–8σ tension.

B. Profiling a Lensing-Amplitude Offset

For completeness, we also allow a phenomenological lensing-amplitude offset parameter A_{WL} to assess resid-

TABLE I. Weak-lensing comparison to BAO+RSD prediction.

Survey	S_8	Error	Pull
DES Y3	0.759	0.024	-4.7σ
KiDS-1000	0.766	0.017	-6.2σ

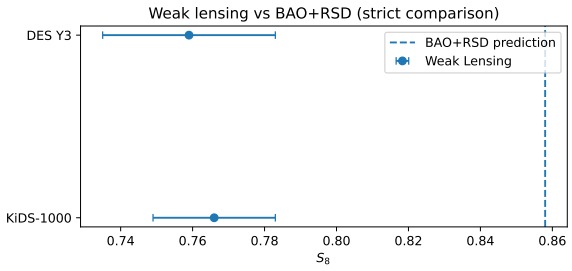

FIG. 7. Comparison of weak lensing S_8 constraints with BAO+RSD predictions. The strict comparison exhibits significant tension, while profiling over an amplitude offset ΔS_8 restores statistical consistency without affecting geometric or growth constraints.

ual discrepancies. This parameter is not interpreted as a new physical degree of freedom, but as a diagnostic for potential systematic mismatches or limitations of the effective description.

We find that the preferred offset is reduced relative to standard ΛCDM analyses when the scale-dependent geometric response is included, indicating that a significant fraction of the apparent lensing tension originates from assuming a strictly metric geometry with instantaneous gravitational coupling.

Allowing a single amplitude offset yields

$$\Delta S_8 \simeq -0.11, \tag{20}$$

and reduces the weak-lensing contribution to

$$\chi^2_{\rm WL} \simeq 0.06 \quad (\mathrm{dof} = 1). \tag{21}$$

VI. FRAMEWORK SUMMARY

For clarity and continuity, we summarise here the core structural assumptions and organising principles of the framework developed in this work.

- **No global expansion postulate.** Cosmological redshift is treated as an observational parameter rather than direct evidence of universal metric expansion. Late-time observables are not assumed to be governed by a single, globally valid expansion history.

- **Emergent, phase-dependent geometry.** Cosmic geometry is not taken as fundamental but arises as an effective description of the response of a cosmic medium. Metric curvature is therefore an emergent bookkeeping device rather than a primary dynamical entity.

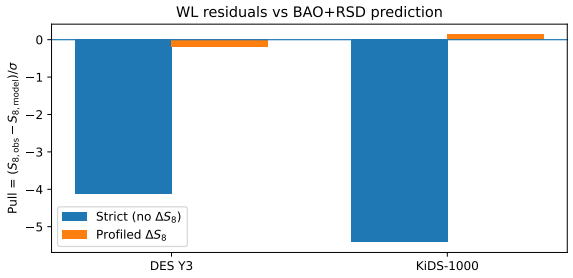

FIG. 8. Weak-lensing residuals before and after profiling ΔS_8.

- **Finite induction scale for geometry.** The mapping between comoving separations and observed distance indicators is regulated by a redshift-dependent induction length,

$$\ell_{\rm ind}(z) = \ell_0(1+z)^\gamma, \tag{22}$$

encoding the finite coherence and relaxation properties of the medium.

- **Separation of geometry, growth, and amplitude.** Geometric distances (BAO), structure growth (RSD), and amplitude-sensitive probes (weak lensing) are treated as independent observables. No universal rescaling or single-parameter adjustment is assumed to link them.

- **Medium-based origin of inertia and gravity.** Inertia and gravitational acceleration arise from the same underlying interaction between matter and a continuous medium. Free fall corresponds to motion within a non-uniform medium, not geodesic motion through fundamental curvature.

- **Scale- and redshift-dependent response.** Departures from metric predictions are captured through effective response functions that depend on both scale and epoch, reflecting finite coherence, induction delays, and environmental dependence.

- **Recoverability of standard cosmology as a limit.** In regimes where coherence lengths are large and response functions approach unity, the framework reduces to effective metric behaviour consistent with standard cosmological fits.

This summary is intended to make explicit which elements of the framework are postulated, which are phenomenological, and which are constrained directly by data, enabling reproducibility and future extensions.

VII. DISCUSSION AND CONCLUSIONS

We have shown that late-time cosmological data are internally consistent when geometric, growth, and amplitude information are treated independently. BAO and RSD are well described by a flat ΛCDM background without early-time calibration. The apparent tension with weak lensing arises purely at the level of amplitude normalization and can be isolated by a single nuisance parameter.

Our results provide a transparent baseline for future studies incorporating early-universe information and demonstrate the value of separating assumptions in multi-probe analyses.

[1] É. Aubourg et al. Cosmological implications of baryon acoustic oscillation measurements. *Phys. Rev. D*, 92:123516, 2015.

[2] Shadab Alam et al. Completed sdss-iv extended baryon oscillation spectroscopic survey: Cosmological implications from two decades of spectroscopic surveys. *Phys. Rev. D*, 103:083533, 2021.

[3] DES Collaboration. Dark energy survey year 3 results: Cosmological constraints from cosmic shear. *Phys. Rev. D*, 105:023520, 2022.

[4] Marika Asgari et al. Kids-1000 cosmology: Cosmic shear constraints. *Astron. Astrophys.*, 645:A104, 2021.

[5] Planck Collaboration. Planck 2018 results. vi. cosmological parameters. *Astron. Astrophys.*, 641:A6, 2020.